

Production Process of Biocompatible Magnesium Alloy Tubes Using Extrusion and Dieless Drawing Processes

Piotr Kustra, Andrij Milenin, Bartłomiej Plonka, and Tsuyoshi Furushima

(Submitted November 19, 2015; in revised form April 19, 2016; published online May 10, 2016)

Development of technological production process of biocompatible magnesium tubes for medical applications is the subject of the present paper. The technology consists of two stages—extrusion and dieless drawing process, respectively. Mg alloys for medical applications such as MgCa0.8 are characterized by low technological plasticity during deformation that is why optimization of production parameters is necessary to obtain good quality product. Thus, authors developed yield stress and ductility model for the investigated Mg alloy and then used the numerical simulations to evaluate proper manufacturing conditions. Grid Extrusion3d software developed by authors was used to determine optimum process parameters for extrusion—billet temperature 400 °C and extrusion velocity 1 mm/s. Based on those parameters the tube with external diameter 5 mm without defects was manufactured. Then, commercial Abaqus software was used for modeling dieless drawing. It was shown that the reduction in the area of 60% can be realized for MgCa0.8 magnesium alloy. Tubes with the final diameter of 3 mm were selected as a case study, to present capabilities of proposed processes.

Keywords dieless drawing process, extrusion, FEM, MgCa0.8, magnesium, optimization

1. Introduction

Metallurgical society has a high demand for modeling and optimization of profile extrusion processes (Ref 1-3). As a consequence, widespread use of FEM (Finite Element Method) in the development of dedicated numerical tools for extrusion simulations can be observed in the scientific literature (Ref 4-6). The Extrusion3d, developed by one of the authors of the paper, is a good example of FEM software for simulation and optimization of extrusion profiles (Ref 7, 8). The software was developed in cooperation with the Quantor company (Ref 9) and was a prototype of the Qform-Extrusion commercial program (Ref 10). Capabilities of Extrusion3d were proven during various research works, see e.g., (Ref 9, 11-13). However, there are also many other commercial FEM codes designed for extrusion modeling, e.g., Forge3, Deform, etc. Peculiarities leading to difficulties in the FEM modeling of extrusion profiles in comparison with modeling of the majority of other three-dimensional forming processes are as follows:

- high number of degrees of freedom in the model due to high gradients of strain rate;
- high mesh sensitivity of obtained results, especially in 3D space;
- excessive computational costs.

Piotr Kustra and **Andrij Milenin**, AGH University of Science and Technology, Mickiewicza 30 Av., 30-059 Krakow, Poland; **Bartłomiej Plonka**, Institute of Non-Ferrous Metals, Light Metals Division in Skawina, Piłsudskiego 19 Av., 32-050 Skawina, Poland; and **Tsuyoshi Furushima**, Tokyo Metropolitan University, 1-1 Minami-osawa, Hachioji, Tokyo 192-0397, Japan. Contact e-mails: pkustra@agh.edu.pl, milenin@agh.edu.pl, bplonka@imn.skawina.pl, and furushimatsuyoshi@tmu.ac.jp.

Mentioned factors caused that application of automatic optimization techniques based on sequential calculations is significantly limited by the computing power. That is why, authors decided to use infrastructure of the supercomputer environment and initiate, at the same time, FE models with different set of parameters and geometries on large number of processors. Utilization of supercomputers network and parallel run of the multiple FE simulations can provide large set of results and identify the best one in the time of a single execution of the model. Such a solution is beneficial when hardly formable materials are investigated and a large number of process conditions have to be tested.

It is well known that magnesium alloys are a good example of materials with low technological plasticity (Ref 14, 15), which is connected with their hexagonal close-packed structure. Recently, the new magnesium alloys containing additions of Ca, Li, and Zn are being intensively developed. These alloys can be used in biomedical applications as, e.g., soluble implants (Ref 16, 17). However, studies on the properties of these alloys have showed that their technological plasticity is even lower than in commercial magnesium alloys (Ref 18, 19). That is why application of numerical modeling to development of robust manufacturing process is required.

Extrusion processes of tubes and profiles from magnesium alloys (as well as other low plastic materials) have specific peculiarities. In addition to the well-known optimization criteria, based on the geometric dimensions of the profile, constraints related to the limited technological ductility of alloys have to be addressed. Development and implementation of appropriate material models to FEM code give an opportunity to account for such constraints (Ref 20, 21).

Meanwhile, a dieless drawing process has been developed in 1969 (Ref 22). This technology can provide great reduction in cross section of, e.g., metal wires, bars and tubes in a single pass. This is possible due to the local heating, which is not used in conventional die drawing processes. Additionally, dieless drawing improves the cleanliness of the tube surface in comparison with the conventional tube drawing because no lubricants are used.

Authors have already successfully fabricated, by the technology, microtubes from superplastic materials with high ductility and low flow stress at elevated temperature (Ref 23, 24). In addition, the dieless drawing process was applied to, typical, AZ31 magnesium alloy tubes (Ref 25). As a result, it was possible to obtain a maximum cross-sectional area reduction of 60% in a single pass of the dieless drawing. In comparison, during the conventional cold die drawing, only 5% reduction in a single pass was possible (Ref 26). Thus, the dieless drawing may be an effective process for fabrication of tubes from typical magnesium alloys. However, no information in the scientific literature can be found on drawing of biocompatible magnesium alloy tubes.

Thus, the aim of the work is numerical identification of process parameters of tubes extrusion and subsequent dieless drawing to obtain defect-free biocompatible tubes made of MgCa0.8 alloy.

2. Numerical Solution of the Boundary Problem in Extrusion

The solution of the boundary problem of extrusion tubes and profiles includes mechanical model, which is based on the theories of plastic flow and heat transfer models. Basic mathematical formulations of the thermo-mechanical solver are as follows:

– equilibrium equations:

$$\sigma_{ij,i} = 0, \quad (\text{Eq 1})$$

– compatibility condition:

$$\xi_{ij} = \frac{1}{2}(v_{i,j} + v_{j,i}), \quad (\text{Eq 2})$$

– constitutive equations:

$$\sigma'_{ij} = \frac{2\bar{\sigma}}{3\bar{\xi}}\xi_{ij}, \quad (\text{Eq 3})$$

– incompressibility equation:

$$v_{i,i} = 0, \quad (\text{Eq 4})$$

– energy balance equation:

$$k(t_{,i})_{,i} + \beta\bar{\sigma}\bar{\xi} = 0 \quad (\text{Eq 5})$$

– yield stress model:

$$\bar{\sigma} = \bar{\sigma}(\bar{\varepsilon}, \bar{\xi}, t), \quad (\text{Eq 6})$$

where σ_{ij} is the stress tensor, ξ_{ij} is the strain rate tensor, v_i is the components of flow vector, σ_{ij} is the deviator of stress tensor, $\bar{\sigma}$, $\bar{\varepsilon}$, $\bar{\xi}$ is the effective stress, effective strain and effective strain rate, respectively, t is the temperature, β is the heat generation efficiency ratio distortion ($\beta = 0.9 \div 0.95$), and k is the thermal conductivity.

Equations 1-4 are converted by the principle of virtual work assumption and techniques to deal with the non-linear FEM algebraic equations, which contain flow velocities and mean stress values as unknown parameters. The frontal method and

iterative calculations of parameter $\mu = \bar{\sigma}/\bar{\xi}$ distribution were used to solve mentioned system of equations. In the solution, interpolation of metal velocity and temperature is based on 15 node prismatic elements, while interpolation of mean stress values is realized by 6 node linear elements. Therefore, the code is based on two different interconnected grids, which are used to solve: heat transfer (T-grid) and mechanical (M-grid) problems, respectively. The latter mesh is significantly finer to provide accurate computational results. To increase the computational efficiency, the code was additionally modified, and the solution of thermal and mechanical problems is realized on two different processors. So, in the parallel mode, heat transfer problem and mechanical problem are solved on separate processors and the exchange of data between T and M grids is possible after completion of both tasks. For details of the presented FEM solutions, refer to earlier authors work (Ref 27).

The optimization process in the present research is based on the multiple execution of the FE model with various sets of process parameters generated by factorial design algorithm. Additionally, the range and the number of intervals of each parameter change were specified. Examples of process parameters that are subjected to evaluation are extrusion velocity, billet temperature, die temperature, pre-chamber temperature, etc. Additionally, the geometrical parameters of the extrusion die were modified in different sets. In the case, user has to prepare several variants of the geometry of the die in a special format compatible with the Qform software (Ref 10).

The key aspect in the present investigation is selection of reliable material models for subsequent large set of calculations.

3. Material Models Used During Calculation

The Hansel-Spittel flow stress model for MgCa0.8 magnesium alloy is introduced in the present research to describe material behavior during deformation:

$$\bar{\sigma} = A \exp(-m_1 t) \bar{\varepsilon}^{m_2} \bar{\xi}^{m_3} \exp\left(\frac{m_4}{\bar{\varepsilon}}\right) (1 + \bar{\varepsilon})^{m_5 t} \exp(m_7 \bar{\varepsilon}) \bar{\xi}^{m_8 t} t^{m_9}, \quad (\text{Eq 7})$$

where A and m_1 - m_9 are empirical coefficients.

Additionally, the failure model was used to predict occurrence of failure instabilities. The model assumes that the fracture is not observed as long as the effective strain is smaller than the critical deformation:

$$\psi = \frac{\varepsilon}{\varepsilon_p(k_\sigma, t, \bar{\xi})} < 1, \quad (\text{Eq 8})$$

where ψ is the ductility function, ε_p is the critical deformation function, k_σ is the triaxiality factor define as $\sigma_0/\bar{\sigma}$, and σ_0 is the mean stress.

Equation 8 is implemented in an integral form:

$$\psi = \int_0^\tau \frac{\bar{\xi}}{\varepsilon_p(k_\sigma, t, \bar{\xi})} d\tau \approx \sum_{m=1}^{m=m_t} \frac{\bar{\xi}^{(m)}}{\varepsilon_p(k_\sigma, t, \bar{\xi})} \tau^{(m)} \quad (\text{Eq 9})$$

where τ is the time of deformation, $\tau^{(m)}$ is the time increment, $\bar{\xi}^{(m)}$ are values of the strain rate in the current time, and m is the index number of time step during numerical integration along the flow line.

According to (Ref 28), the critical deformation can be expressed as a function of stress triaxiality, temperature t , and effective strain rate $\dot{\xi}$:

$$\varepsilon_p(k_\sigma, t, \dot{\xi}) = d_1 \exp(-d_2 k_\sigma) \exp(d_3 t) \dot{\xi}^{d_4}, \quad (\text{Eq 10})$$

where d_1 - d_4 are empirical coefficients.

To increase model predictive capabilities, two conditions to avoid material damage during processing were introduced: maximum value of ductility function (8) has to be less than one and maximum calculated temperature has to be less than the incipient melting temperature of MgCa0.8 alloy, which is 516 °C.

Presented flow stress and failure models were then properly identified based on a series of experimental tests.

4. Identification of Material Models Parameters

Mentioned flow stress and fracture models for MgCa0.8 (Mg 99.2 wt.%, Ca 0.8 wt.%) alloy were identified via a series of experimental investigations involving upsetting and tension tests. First, the material was casted in an argon atmosphere to ingot mold with diameter 130 mm. Then, extrusion process from diameter 130 to 20 mm was performed at 400 °C. Due to the large deformation during extrusion, the texture of material is axially oriented. The texture of cross section of extruded rod is presented in Fig. 1. Samples for upsetting and tension tests (Fig. 1) were cut out from the extruded rod. For compression test, a cylindrical specimen with diameter of 8 mm and height of 10 mm was used. Upsetting and tension tests were performed on the Zwick Z250 machine at the AGH University of Science and Technology. Results of the compression tests were used to determine the flow stress model and results of both tests were used for identification of fracture (workability) model. Conditions and results of the experiment are shown in Table 1.

As presented, for the compression samples 1, 2 as well as tension sample 1 (Table 1), the fracture has not occurred.

Then coefficients in Eq 7 were determined using the inverse approach (Ref 20) with the least squares method. The objective function was formulated as the root-mean-square difference

between experimental and predicted loads. The following values of coefficients were obtained: MgCa0.8: $A = 405.85$; $m_1 = -0.00826428$; $m_2 = -0.0281807$; $m_3 = 0.020492$; $m_4 = -0.0114059$; $m_5 = 0.00521939$; $m_7 = -0.69316$; $m_8 = 0.0001636$; $m_9 = 0.192958$.

Parameters d_1 - d_4 in Eq 10 were obtained from fracture tests for different values of k_σ , t , $\dot{\xi}$. Interpretation of results of tensile and upsetting tests was done using the inverse algorithm (Ref 20). The FEM models of all tests were made for determining conditions of fracture initiation (k_σ , t , $\dot{\xi}$). Changes in values k_σ , t , $\dot{\xi}$ during deformation were calculated in that part of the sample, where initiation of fracture occurred in the tests. The ductility function for each test was calculated on the basis of Eq 9 and 10. The difference between measured and calculated values of ductility function at the moment of the fracture was used as the objective function. The following values of coefficients were obtained: $d_1 = 0.04611$; $d_2 = 0.4759$; $d_3 = 0.01265$; $d_4 = -0.07009$ (Ref 20).

5. Development of Extrusion Process of MgCa0.8 Tube

Based on the developed code and identified material models, the optimization of extrusion process parameters of MgCa0.8 alloy tubes was performed. The experimental part was carried out in the Institute of Non-Ferrous Metals in Skawina (Poland). Figure 2 shows schematically the extrusion die, with a chamber designed to reduce the force during extrusion. Illustration of tools assembly is shown in Fig. 3.

Extruded tube had diameter of 5 mm (internal diameter 4 mm). A diameter of rod was 20 mm and extrusion velocity was set to 1 mm/s. The reason for optimizing the thermal conditions in extrusion process was formation of defects (cracks) in the final tube (Fig. 4). Therefore, the optimization of billet temperature was performed. Examples of results obtained for the billet temperature of 400, 350, 300 °C and container temperature of 380, 370, 350 °C are shown in Fig. 5, 6, and 7, respectively.

Obtained results for billet temperature of 400 °C allow to conclude that the ductility function reaches value less than one

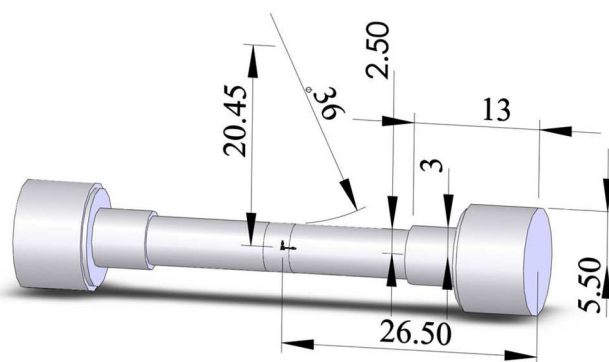
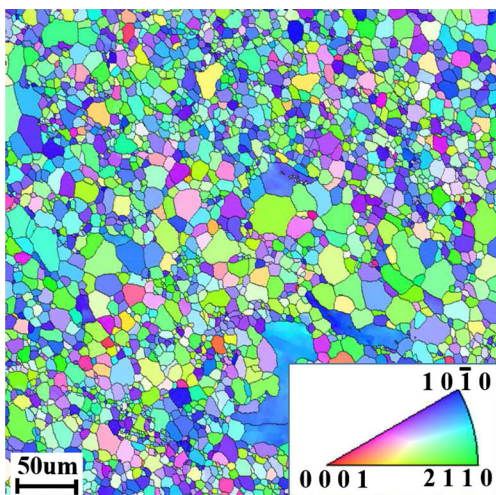



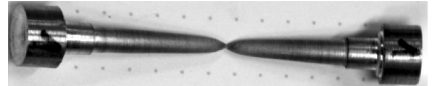

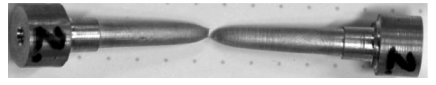

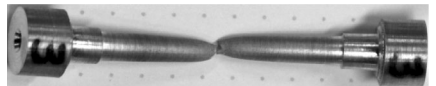

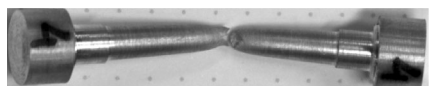


Fig. 1 Texture of cross section of extruded rod, shape and dimensions of the sample for tension tests

Table 1 Conditions and results of tension and compression tests

Sample	t , °C	v , mm/s	Deformation, mm		C	T
			C^a	T^a		
1	400	10	7.3	...		
2	300	1	5.8	23		
3	300	10	5.6	16		
4	250	1	6.1	14		
5	250	10	4.7	8.5		

C compression, T tension, t temperature, v tool velocity

^aThe deformation, which corresponds to destruction of sample, mm

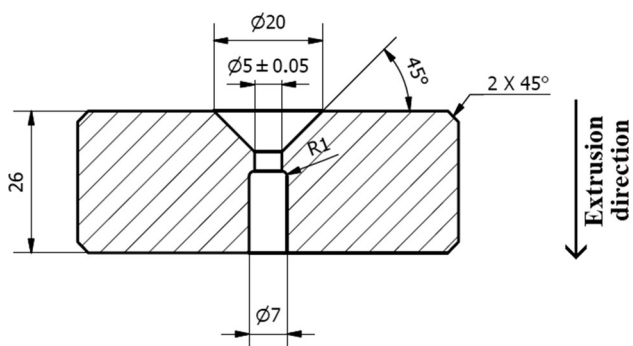


Fig. 2 Shape and dimensions of extrusion die

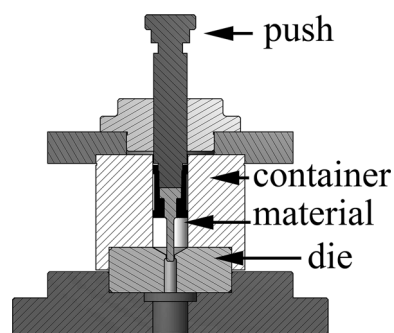


Fig. 3 Extruding tools assembly, the Institute of Non-Ferrous Metals in Skawina

(Fig. 5). It is worth noting that dependence of tube temperature after extrusion on billet temperature has non-linear character. By lowering the billet temperature, heat generation increases and

more intense temperature rise can be observed. Eventually, based on the selected variant of extrusion process, the tube without defects was manufactured during experiment as shown in Fig. 8.

The tubes are subsequently subjected to dieless drawing process to obtain required dimensions of the final product.

6. Development of Dieless Drawing Process of MgCa0.8 Tube

Tubes dieless drawing process with local heating and tensile deformation is a flexible drawing technique where no dies are present during deformation. Figure 9 shows a schematic illustration of dieless drawing process, in which heating

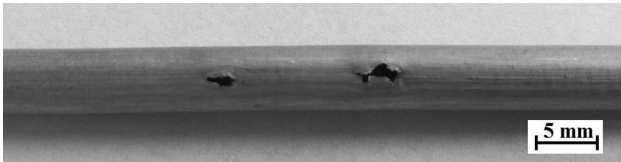


Fig. 4 An example of the formation of defects during the tube extrusion in temperature 350 °C

devices are fixed and the tube moves from left to right through the heating zone. The tube is subjected to tension by the difference in speed before and after deformation zone: V_1 and V_2 . The necking occurs at locally heated area and diffuses with moving the tube under tension. The relationship between the reduction in area R and the speed ratio V_2/V_1 is as follows:

$$R = 1 - \frac{A_1}{A_0} = 1 - \frac{V_2}{V_1}, \quad (\text{Eq 11})$$

where A_0 is the original cross-sectional area and A_1 is the cross-sectional area after the drawing.

Numerical model of dieless drawing was developed in the commercial Abaqus software. Again, Eq 7 was used as the flow stress model. As the melting point of MgCa0.8 magnesium alloy is 516 °C, the temperature of heating element was set below that critical value and was equal 450 °C. Additionally, two more tensile tests were performed for 450 °C and the strain rates of 0.1 and 0.01 s⁻¹ to cover the whole range of possible temperatures and strain rates. Initial temperature of tube was 20 °C and the feeding speed V_2 was fixed at 0.1 mm/s and the tensile speed V_1 was controlled to adjust reduction in the area R . Numerical simulations were carried out for different lengths

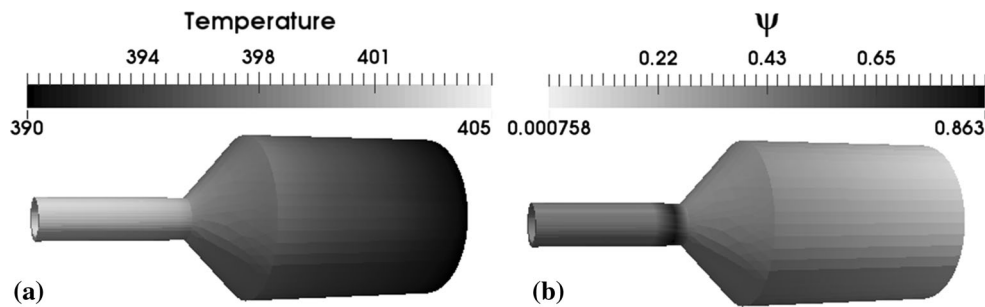


Fig. 5 Temperature distribution (a) and distribution of ductility function (b) for the billet temperature of 400 °C (Option 1)

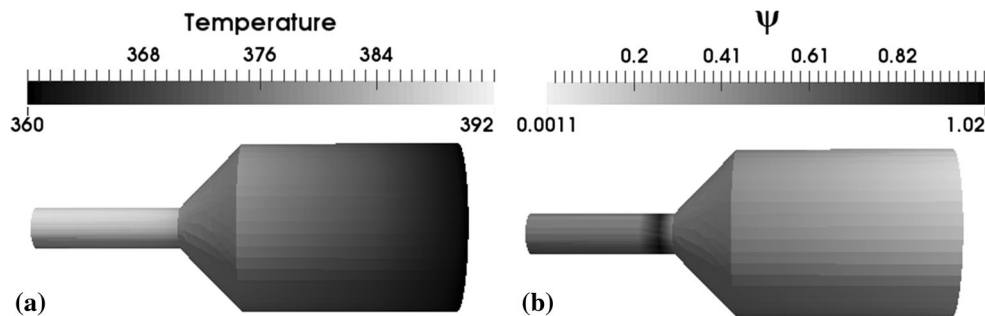


Fig. 6 Temperature distribution (a) and distribution of ductility function (b) for the billet temperature of 350 °C (Option 2)

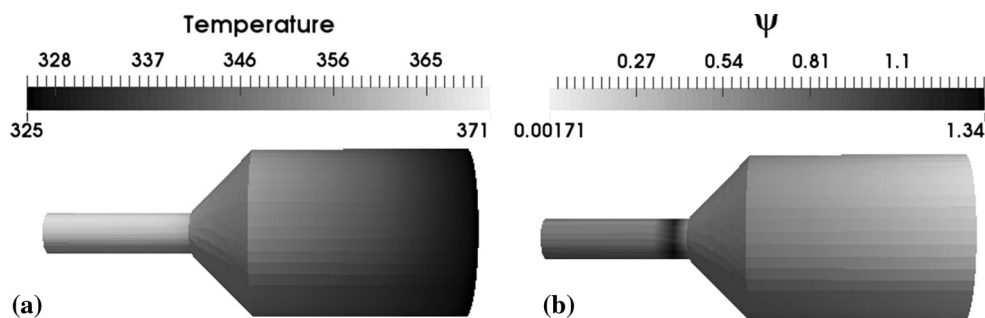


Fig. 7 Temperature distribution (a) and distribution of ductility function (b) for the billet temperature of 300 °C (Option 3)

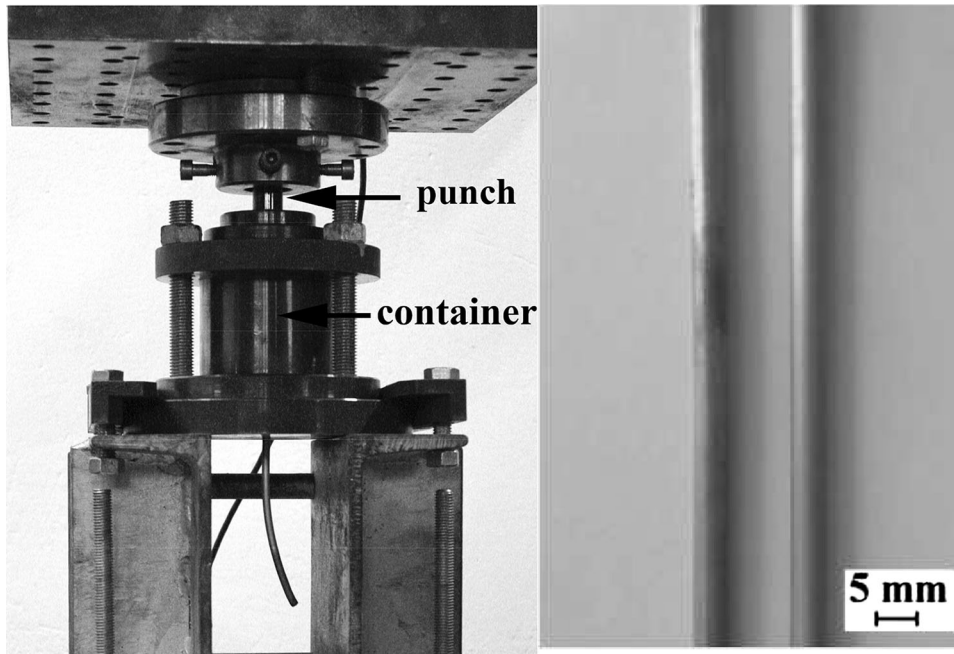


Fig. 8 Extrusion equipment and tube made from MgCa0.8 alloy obtained experimentally in the extrusion process for the conditions corresponding to numerical calculations (Option 1)

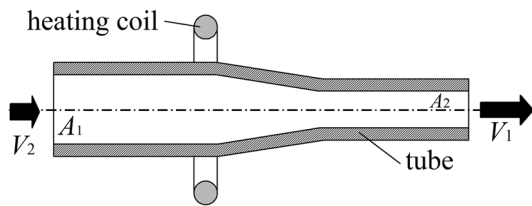


Fig. 9 Schematic illustration of dieless drawing process

of heating element and two reductions of 41 and 60%, respectively. Results of simulations are shown in Fig. 10 and 11. It can be observed that length of heating element and deformation ratio has a significant impact on the tube diameter and wall thickness in dieless drawing process. Increase of reduction R (Eq 11) during the process results in decrease of tube wall thickness and decrease of external tube diameter because deformation is higher. Increase of the length of heating element causes that tube cross section has more time for deformation during passing through the heating zone. That is why external diameter of tube is lower. Thus, it is clear from

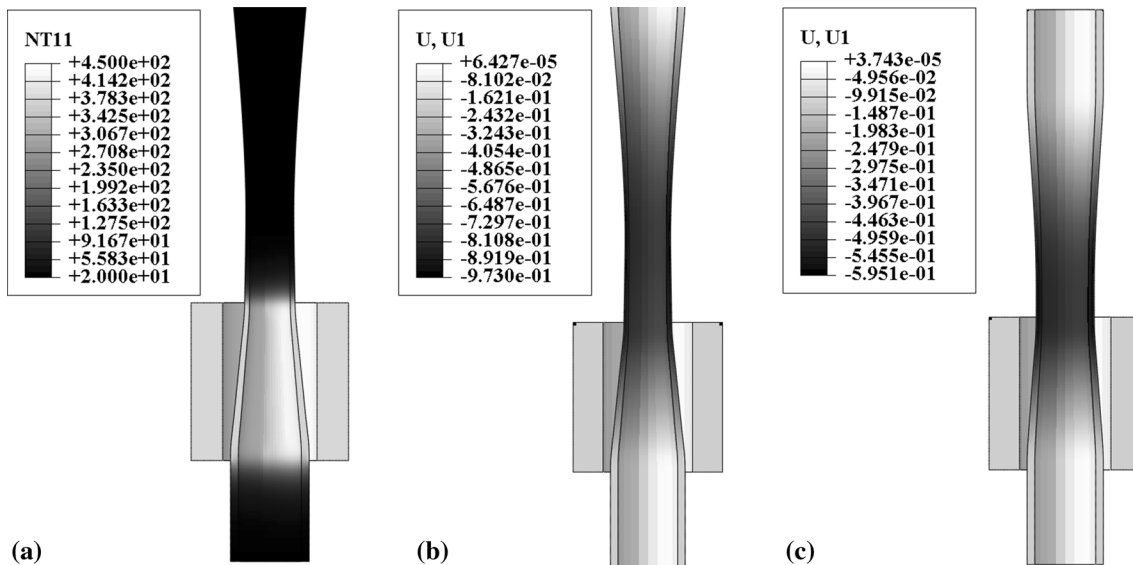


Fig. 10 Results of numerical simulation at the cross section of pipe for length of heating element equal to 10 mm: (a) distribution of temperature for $R = 60\%$, (b) distribution of displacement for $R = 60\%$, (c) distribution of displacements for $R = 41\%$

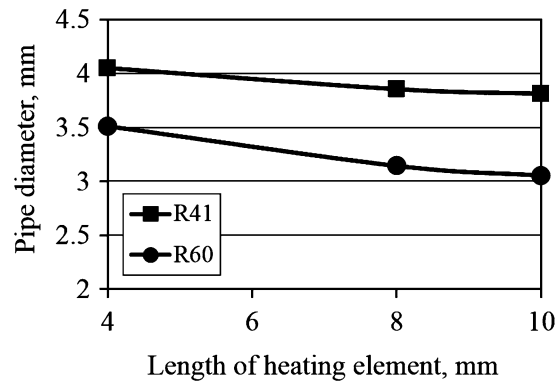
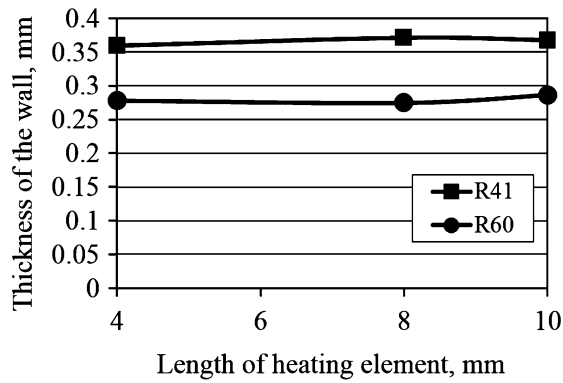


Fig. 11 Results of numerical simulation of drawing process for different lengths of heating element

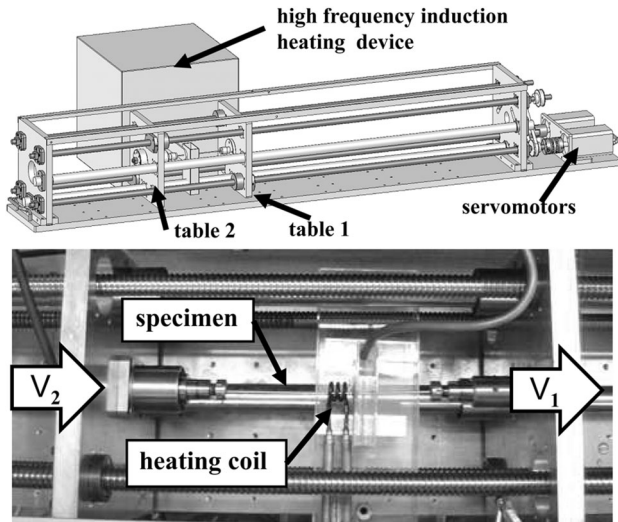


Fig. 12 Scheme (top) and photo (bottom) of the experimental setup of dieless drawing process

power of 2 kW and a frequency of 2.2 MHz was used as the heat source for the specimens. The temperature inside the heating coil was measured with a non-contact two-color pyrometer. In the experiment, the heating temperature was the same as in simulations and was set as 450 °C. The feeding speed V_2 was fixed at 0.1 mm/s and also two reductions were examined—41 and 60%.

Figure 13 shows the photograph of deformed tubes after dieless drawing process in a single pass. Reduction in area and outer diameter after the drawing process can be obtained without using any tools and dies by controlling speed ratio V_2/V_1 . In this experiment, maximum reduction in the area of 60% can be realized for MgCa0.8 magnesium alloy. Using this result, the validity of dieless drawing process for biocompatible MgCa0.8 magnesium alloy can be verified experimentally.

In the experiment, the length of the heating zone was approximately equal to 10 mm. Results of numerical simulation were close to those in the physical drawing process. For reduction 41% in experimental process, diameter of the tube was 3.5 mm and in simulation was 3.81 mm. Adequately, for reduction 60% diameters of tube were 3 and 3.05 mm, for physical experiment and simulation, respectively.

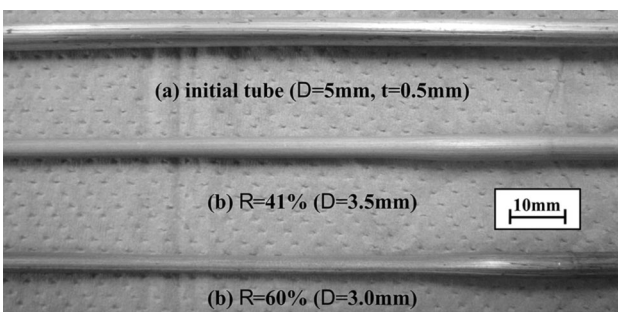


Fig. 13 Photograph of deformed tubes after dieless drawing process in a single pass under a condition of heating temperature of 450 °C

numerical simulations that the length of heating element has no significant effect on the tube wall thickness.

Numerical investigation provided valuable information for experimental research on the dieless drawing device. Figure 12 shows the scheme and photograph of the experimental setup of dieless drawing process used in the present study. A tensile speed V_1 applied to the tube and a feeding speed V_2 can be independently controlled, following Eq 11, using two servo motors. A high-frequency induction heating device with a

7. Conclusions

1. The new process for production of thin tubes from biocompatible magnesium alloy was presented. This process consists of two stages—extrusion and dieless drawing process.
2. The proposed concept of optimization of extrusion process of Mg alloys is based on numerical simulations realized in a parallel mode. This gave the opportunity to solve the optimization task in a time of a single simulation.
3. Experimental verification of the model was performed on the basis of experimental extrusion process of biocompatible tubes made of MgCa0.8 alloy. In extrusion process, magnesium tubes without defects were obtained.
4. Extruded tubes were used as an input for dieless drawing process. Experiment showed that for MgCa0.8 alloy it is possible to reduce cross section of the tube to 60%, which is significantly larger than that of 5% in a single pass of cold drawing.
5. Numerical simulation showed that during dieless drawing process, the length of heating element and drawing velocity has an effect on radius and wall thickness of the tube.

That is why optimization of this process is possible. It is also possible to obtain tube with variable cross section and wall thickness.

Acknowledgments

This research was supported in part by PL Grid Infrastructure, Financial assistance from the NCBiR of Poland, Project No. V4-Jap/2/2016 is acknowledged.

References

1. P. Machado, Extrusion die design, *Proceeding of Fifth International Extrusion Technology Seminar*, Vol. 1, May 19–22, 1992 (Chicago, USA), p. 385–389
2. M. Kiuchi, J. Yanagimoto, and V. Mendoza, Three-Dimensional FE Simulation and Extrusion Die Design, *J. Jpn. Soc. Technol. Plast.*, 1998, **39**, p 27–32
3. J. Herberg, K. Gundeso, and I. Skauvic, Application of Numerical Simulation in Design of Extrusion Dies, *6 International Aluminium Extrusion Technology Seminar*, May 14–17, 1996 (Chicago, USA), p 275–281
4. J.L. Chenot and F. Bay, An Overview of Numerical Modeling Techniques, *J. Mater. Process. Technol.*, 1998, **80–81**, p 8–15
5. J.L. Chenot, Recent Contributions to the Finite Element Modelling of Metal Forming Processes, *J. Mater. Process. Technol.*, 1992, **34**, p 9–18
6. B.J.E. Rens, W.A.M. Brekelmans, and F.P.T. Baaijens, A Semi-Structured Mech Generator Applied to Extrusion, *Proceedings of the 7 International Conference on Numerical Methods in Industrial Forming Processes*, J. Huetink, F.P.T. Baaijens, Ed., Jun 22–25, 1998 (Enschede, Netherlands), p 621–626
7. A. Milenin, Mathematical Modeling of Operations of Correcting the Dies for Section Extruding., *Metallurgicheskaya i Gornorudnaya Promyshlennost*, 2000, Vol. 1–2, p 64–66 (**in Russian**)
8. A. Milenin, S. Berski, G. Banaszek, and H. Dyja, Theoretical Analysis and Optimization of Parameters in Extrusion Process of Explosive Cladded Bimetallic Rods, *J. Mater. Process. Technol.*, 2004, **157–158**, special issue, p 208–212
9. A.I. Lishnij, N.V. Biba, and A. Milenin, Two Levels Approach to the Problem of Extrusion Optimization, Simulation of Materials Processing: Theory, Methods and Applications, *Proceedings of the 7 International Conference on Numerical Methods in Industrial Forming Processes*, J. Huetink, and F.P.T. Baaijens, Ed., Jun 22–25, 1998 (Enschede, Netherlands), p 627–631
10. N. Biba, S. Stebunov, A. Lishny, and A. Vlasov, New Approach to 3D Finite-Element Simulation of Material Flow and its Application to Bulk Metal Forming, *7th International Conference on Technology of Plasticity*, Oct. 27–Nov. 1, 2002 (Yokohama, Japan), 2, p 829–834
11. A. Milenin, Modelowanie Numeryczne Procesów Wyciskania Profili z Zastosowaniem Gęstości Dyslokacji jako Zmiennej Wewnętrznej w Modelu Reologicznym Materiału, *Informatyka w Technologii Materiałów*, 2002, **1(2)**, p 26–33 (**in Polish**)
12. A.I. Lishnij, N.V. Biba, and A.A. Milenin, Two Levels Approach to the Problem Of Extrusion Optimization, Simulation of Materials Processing: Theory, Methods and Applications, *Proceedings of the 7 International Conference on Numerical Methods in Industrial Forming Processes*, J. Huetink, and F.P.T. Baaijens, Ed., Jun 22–25, 1998 (Enschede, Netherlands), p 627–631
13. A. Milenin, A.N. Golovko, and I. Mamuzic, The Application of Three-Dimensional Computer Simulation when Developing Dies for Extrusion of Aluminium Shapes, *Metallurgija*, 2002, **41(1)**, p 53–55
14. N. Odawa, M. Shiomi, and K. Osakada, Forming Limit of Magnesium Alloy at Elevated Temperatures for Precision Forming, *Int. J. Mach. Tools Man.*, 2002, **42**, p 607–614
15. K. Yoshida, Cold Drawing of Magnesium Alloy Wire and Fabrication of Microscrews, *Steel Grips.*, 2004, **2**, p 199–202
16. H. Haferkamp, V. Kaese, M. Niemeyer, K. Phillip, T. Phan-Tan, B. Heublein, and R. Rohde, Exploration of Magnesium Alloys as New Material for Implantation, *Materialwiss. Werkst.*, 2001, **32**, p 116–120
17. M. Thomann, Ch Krause, D. Bormann, N. Von der Höh, D. Windhagen, and A. Meyer-Lindenberg, Comparison of the Resorbable Magnesium Alloy LAE442 an MgCa0.8 Concerning Their Mechanical Properties, Gradient Degradation and Bone Implant-Contact after 12 Month Implantation in Rabbit Model, *Materialwiss. Werkst.*, 2009, **40(1–2)**, p 82–88
18. A. Milenin, D. Byrska, and O. Gridin, The Multi-Scale Physical and Numerical Modelling of Fracture Phenomena in the MgCa0.8 Alloy, *Comput. Struct.*, 2011, **89**, p 1038–1049
19. A. Milenin, D.J. Byrska, O. Grydin, and M. Shaper, The Experimental Research and the Numerical Modeling of the Fracture Phenomena in Micro Scale, *Comput. Methods Mater. Sci.*, 2010, **10**, p 61–68
20. A. Milenin, M. Gzyl, T. Rec, and B. Plonka, Computer Aided Design of Wires Extrusion from Biocompatible Mg-Ca Magnesium Alloy, *Arch. Metall. Mater.*, 2014, **59**, p 551–556
21. A. Milenin and P. Kustra, Numerical and Experimental Analysis of Wire Drawing for Hardly Deformable Biocompatible Magnesium Alloys, *Arch. Metall. Mater.*, 2013, **58**, p 55–62
22. V. Weiss and R.A. Kot, Dieless Wire Drawing with Transformation Plasticity, *Wire J.*, 1969, **9**, p 182–189
23. T. Furushima and K. Manabe, Experimental Study on Multi-Pass Dieless Drawing Process of Superplastic Zn-22 % Al Alloy Microtubes, *J. Mater. Process. Technol.*, 2007, **187–188**, p 236–240
24. T. Furushima, A. Shirasaki, and K. Manabe, Fabrication of Noncircular Multicore Microtubes by Superplastic Dieless Drawing Process, *J. Mater. Process. Technol.*, 2014, **214**, p 29–35
25. T. Furushima, and K. Manabe, Workability of AZ31 Magnesium Alloy Tubes in Dieless Drawing Process, *Steel Res. Int.*, special issue, 2012, p 851–854
26. K. Yoshida and A. Koiwa, Cold Drawing of Magnesium Alloy Tubes for Medical, *ASME 2011 International Manufacturing Science and Engineering Conference*, June 13–17, 2011 (Corvallis, Oregon, USA), p 541–545
27. M. Kopernik and A. Milenin, Two-Scale Finite Element Model of Multilayer Blood Chamber of POLVAD_EXT, *Arch. Civ. Mech. Eng.*, 2011, **12(2)**, p 178–185
28. J.L. Chenot, L. Fourment, T. Coupez, R. Ducloux, and E. Wey, Forge3—A General Tool for Practical Optimization of Forging Sequence of Complex Three-Dimensional Parts in Industry, *International Conference on Forging and Related Technology*, 1998, Suffolk, UK, p 113–122